In-situ and in-operando Grazing Incidence XAS: a novel set-up and its application to model Pd electrodes for alcohols oxidation.

E. Berretti[a,b], A. Giaccherini[c], V. Dell'Aquila[d], F. Di Benedetto[e], G. Montegrossi[f], G. O. Lepore[g], M. Innocenti[d], F. D'Acapito[h], F. Vizza[a,*], A. Lavacchi[a].

[a] *CNR- ICCOM, Institute for the chemistry of Organometallic Compounds, Via Madonna del Piano n.10, Sesto Fiorentino, 50019, Italy*
[b] *INSTM, National Interuniversity Consortium of Materials Science and Technology, Via G. Giusti n.9, 50121 Firenze, Italy*
[c] *Industrial Engineering Department (DIEF), University of Florence, Via di S. Marta n.3, 50139, Firenze, Italy*
[d] *Chemistry Department, University of Florence, Via della Lastruccia n.3, Sesto Fiorentino (Florence) 50019, Italy*
[e] *Department of Physics and Earth Science, University of Ferrara, Via Saragat n.1, 44122, Ferrara, Italy*
[f] *CNR-IGG, Institute of Geosciences and Earth resources, Via Giuseppe Moruzzi n.1, 44121, Pisa, Italy*
[g] *Earth Sciences Department (DST), University of Florence, Via Giorgio la Pira n.4, 50121, Firenze, Italy*
[h] *CNR-IOM-OGG, Materials Foundry, ESRF, Avenue des Martyrs 71, 38043, Grenoble, France*
* *Corresponding author*

Abstract: In this article, we present an *in-situ* and *in-operando* time-resolved X-ray Absorption Spectroscopy (XAS) technique which exploits a combination of Grazing Incidence XAS (GIXAS) and Fixed Energy X-Ray Absorption Voltammetry (FEXRAV), the Grazing Incidence FEXRAV (GI-FEXRAV). A case-study is also outlined. Palladium ultra-low loadings were deposited above Au polycrystalline iso-oriented substrates adopting three different deposition methods: surface-controlled electrochemical methods, direct electrodeposition and physical vapour deposition. These catalytical surfaces were prepared for the investigation by GI-FEXRAV of the Pd oxidation/dissolution phenomenon that could occur when the metal is used in the anodic compartment of Direct Alcohol Fuel Cells (DAFCs) or in electrochemical reformers. Moreover, we report a robust, low cost and versatile procedure to obtain wide and flat iso-oriented gold substrates that can mimic monocrystalline gold (1 1 1) in the electrochemical response. The use of GI-FEXRAV for the *in-operando* characterization of the catalysts, in conjunction with the designed experimental cell and our flexible Au-based electrochemical substrates show an invaluable potential in the in-*operando* study of fundamental phenomena in heterogeneous electrocatalysis model systems and, due to itsversatility, paves the way to further studies on a wide selection of electrochemical systems.

1. INTRODUCTION

Electrocatalysis is subject to an ever-growing research interest, being one of the driving forces of the green revolution, the global effort which will lead to a change of paradigm from today's fossil fuels consumption to low-cost energy availability from renewable sources. Specifically, electrochemical conversion of alcohols and Small Organic Molecules (SOM) in direct liquid fuel cells (FCs) or in electrochemical reformers is now under the spotlight for its potential impact in energy conversion and storage [1–7]. A successful implementation of FCs technologies will require the optimization of the electrode materials, to achieve both performance and stability [8]. It is undoubted that, in order to permit the widespread diffusion of such devices, a major research effort is required to decrease electrocatalysts load and increase its durability (especially when using elements which are considered as critical raw materials[9]). For these reasons it is paramount to develop efficient techniques to characterize the reactions occurring on the electrocatalysts surfaces in operative conditions.

Many techniques are proposed today for the study of the performance of electrochemical conversion devices. Among them, time resolved electrochemical XAS methods are promising because X-rays are able to probe selectively the chemical evolution of single elements, even if inside complex matrices like in real devices. XAS is particularly useful for the study of heterogeneous electrocatalysts, like metallic nanoparticles [8,10–13], or for atomically dispersed electrocatalysts like the XPc systems (X=Fe,Ni,Co). [14–19] Specifically, some XAS methods permit a better understanding of the nature and kinetics of the processes occurring at the surface of an electrode, by probing its fast operando changes. As an example, quick-XAS could permit a rapid acquisition of portions of the absorption spectra during electrochemical stimulus, but it is not implemented in every XAS beamline. [20] On the contrary Fixed Energy X-Ray Absorption Voltammetry (FEXRAV) [21] can be easily adopted in every synchrotron XAS line, despite its loadout. FEXRAV is an operando technique that exploits a fixed energy XAS acquisition on the working electrode during a potential variation of an electrochemical (EC) cell, enabling the acquisition of kinetic data on the evolution of chemical systems subjected to electrical stimulus. The technique can probe selectively one element at a time, even in complex matrices, by giving time resolved information on the speciation and/or structure evolution of that element and its surrounding atoms. FEXRAV has already demonstrated its usefulness as a tool to study the chemical behavior of electrocatalysts during duty cycles. Studies on Fe, Ag and Ir oxidation [21–23] are present in literature. The use of such technique in our group was, in the past, devoted to the characterization of palladium deactivation phenomenon in direct ethanol and formate FCs, both in half-cell [24,25] and working fuel cell [26] configurations. By increasing anodically the potential of the working electrode, we were able to follow: 1) the oxidation of the Palladium on the surface of the electrocatalyst [27,28] and 2) its dissolution in form of hydroxipalladiates [24]. In these experiments, we exploited a powdered catalyst composed by palladium nanoparticles dispersed in a carbon matrix [29], a benchmark of the systems commonly used in fuel cell stacks. Despite being real systems, nano-dispersed catalysts represent a challenge for live-characterization. As an example, due to the complexity of their surfaces, it is difficult to perform identical location studies at different stages of their working life, and thus to correlate variations in their performances with precise changes occurring in a precise region of the electrocatalysts. Moreover, XAS is a bulk technique, which is able to sample a material in all its depth. This makes XAS an effective technique for high surface-to-volume samples, like nanoparticles systems, the smallest the particles the better. Limitations to this approach could in fact arise when the abovementioned ratio decreases. Let us consider as an example a unimodal dimensional distribution of spherical nanoparticles subjected to electrochemical stimulus as a working electrode. Only a portion of the nanoparticles, the outer shell, participates in the electrochemically induced reactions, while the core remains unmodified during the process. Still, the incident X-rays sample all the catalyst volume. The obtained XAS absorption signal will be then mediated; a small portion of the absorption signal will be due to the chemical changes occurring on the element of choice at the surface, while a usually bigger portion of the signal will be caused by the absorption from core of the particles, unaffected by the electrochemical stimulus. It is consequently easy to understand that the extent of this mediation effect will be dependent on the particle size. Big particles will lead to lower surface-to-bulk signal ratios, increased acquisition time and decreased chance to probe fast speciation changes at the electrochemical interface, ultimately rendering this method unfeasible for the study of fast kinetic systems. On the contrary, by decreasing the nanoparticles dimensions we'll increase the overall electroactive volume, and thus the surface-to-bulk signal ratio.

The aim of this research was to push this concept to the limit, by proposing a technique enabling the XAS characterization of ultra-thin layers of catalyst deposited on a flat surface, where the absolute majority of the surface atoms participate to the electrochemical changes occurring at the surface. Specifically, we propose a case-study which connects whit our previous studies on Pd and FEXRAV. [24–26] We produced ultra-low loading Palladium films of different thicknesses on polycrystalline iso-oriented Au (111) base-substrates. Pd and Pd-Au alloys are extremely efficient in the electrochemical conversion of alcohols and SOM in direct liquid FCs [3,30–36]; nevertheless, they show limitations in the performance along with the limited stability under strong anodic overpotentials that can sometimes occur in DAFCs [37,38]. One of our goals was to probe Pd-Au surfaces stability toward bare alkaline electrolyte, like the base electrolyte used in DAFCs. Our previous studies [24–26] in which FEXRAV was adopted in half-cell and fuel-cell configurations, demonstrated that the use of fuel-containing alkaline electrolyte (Fuel = Ethanol, Formate) produces a decrease in performance under oxidative potentials, but hinders Pd dissolution from the working electrode. Hence, our purpose to use bare alkaline electrolyte puts ourselves in the worst-case scenario in which both oxidation and dissolution co-exist, In addition, we used a flat submonoatomic-like catalytical architecture in which the vast majority of the Pd atoms participate to the electrochemical reactivity.

In summary, in the present article, we report:

1) the procedure to prepare the Au polycrystalline iso-oriented (111) surfaces, to be used as base electrodes for the growth of different electrocatalyst layers. These surfaces show a high degree of reproducibility, robustness, and an electrochemical response which mimics the one that can be expected for monocrystalline (111) gold surfaces;

2) the adopted experimental set-up for Grazing Incidence FEXRAV, comprising the cell design and the acquisition settings and geometry and

3) a case study for the application of the GI-FEXRAV, where palladium was grown into different thicknesses on the Au iso-oriented surfaces, and tested towards oxidative stress in bare alkaline solution.

The variation of Pd deposit depth permitted to explore the limits of the technique. Moreover, to the best of our knowledge, no trace of large base electrodes as the ones presented in this article is available in literature, especially taking into consideration such defined response towards surface-limited electrochemical processes. The versatility of these substrates, in conjunction with the GI-FEXRAV technique, paves the way to the operando characterization of a vast variety of different electrocatalysts.

2. EXPERIMENTAL

2.1. Polycrystalline Iso-oriented Au (111) substrate preparation and characterization

2.1.1. *Electrode production*

Wide polycrystalline Gold (1 1 1) substrates were prepared using sputtering methods, by deposition of two metals onto glass microscope slides (Supplied by Agar Scientific). The glass surfaces were used as a cheap inert support for the deposition of the metals, due to their wide surface (3x1 inches) and certified continuous flatness (within .00011″ per inch). Prior to deposition, glass slides were cleaned by the following cycle: a) a 10 minutes sonication cycle in Acetone (technical grade), b) rinsing using milli-q water, c) a 10 minutes sonication cycle in EtOH 99.9% d) rinsing using milli-q water and e) drying under nitrogen flux. A magnetron sputtering device for the preparation of Scanning Electron Microscopy (SEM) samples, an EMITECH K575X Turbo Sputter Coater was used to produce: a) a 150 nm thick tantalum deposit above glass as bond coat and b) a 70 nm thick gold deposit above tantalum. Metallic layer thicknesses were determined by measuring the weight of some test deposits on a glass slide surface; for the calculus, a homogeneous growth of the films on the surface was considered. Thickness of the layers was defined a priori in order to minimize ohmic drop of the electrodes. Base substrates were produced with two different coverages: a) full slide coverage, for the electrochemical tests, and half-slide coverage for the XAS experiment (Figure 1). This second coverage variation, obtained by simple masking of the glass slide during the PVD process, was needed in order to prevent current overflow of the potentiostat during FEXRAV experiments. For the sputtering process, a Ta 99,99% disk (Goodfellow) and an Au 99,99% foil (Goodfellow) were used as targets; Argon was adopted as process gas for both the physical vapor processes.

Once prepared, the deposits were heat treated to favor the surface rearrangement of the (1 1 1) oriented surface [39]. We tested two different annealing procedures: oven- and flame annealing. Oven annealing was performed using an electric oven (Nabertherm) with the following heating cycle: 1) heating from 25°C to 600°c in 1 hour, 2) 3 to 6 hours at 600 °C, cooling from 600°C to 25°C in 2 hours. During the whole process, oven chamber was fluxed with N2. Flame annealing process was performed placing the glass slides face up on a thick copper surface and by designing slow inward spirals toward the surface whit a butane flame, in order to minimize thermal shock. We observed a precise reproducibility of the electrochemical measurements only in the surfaces in which no change in brightness or reflectivity was visible after the annealing process, both for oven and flame annealing.

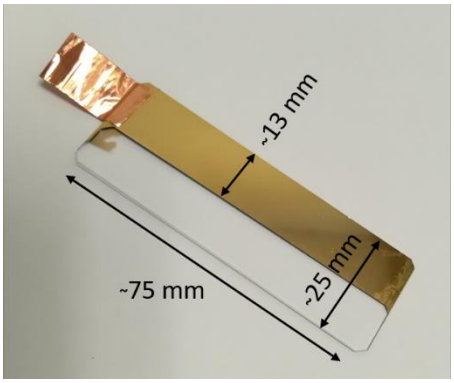

Figure 1 – Appearance of a substrate just before its use in the GI-FEXRAV experiment. In the image the overall dimensions are also reported

2.1.2.Electrode characterization

Surface morphology was investigated using a TESCAN GAIA 3 FIB/SEM. Images of the surface were acquired in beam deceleration mode (BDM) using a landing energy of 2 keV and a low beam current (25 pA).

AFM was also performed on the various sample surfaces prior and after the annealing procedures using a MFP3D Asylum Research AFM, in order to define changes in surface roughness. For each different heat-treated batch, 4 different samples were analyzed by performing three AFM acquisitions at the sides and in the center of the glass slide. Roughness data were extracted from AFM images using Gwyddion software [40] and mediated in and between the batches.

2.2. Pd thin film deposition and characterization

Three different palladium deposition processes were used in this study: 1) an electrochemical surface-controlled procedure to produce an ultra-low loading of Pd on the surface of the Au electrodes, 2) a direct electrochemical (galvanostatic) palladium deposition and 3) a Physical Vapor Deposition of Pd onto the electrodic surfaces. The preparation methods will be described in the following sections. Both the electrochemical depositions were performed inside the designed cell (2.3.2) using a Par 2263 Potentiostat/Galvanostat. Pd surface testing was performed using two different electrolytic solutions: a) NaOH 1M (Sigma Aldrich) + EtOH 1M (AnalaR Normapur 99,9%, WWR Chemicals) for the comparison of the electrochemical response between the different palladium loadings and b) NaOH 2M (Sigma Aldrich) for the in-situ XAS experiments.

2.2.1. Ultra-low loadings of Pd on Au from electrochemical UPD+SLRR

For the production of the ultrathin deposit of palladium, we used a two-step method, consisting in Under Potential Deposition (UPD) + Surface Limited Redox Replacement (SLRR) [41,42]. Particularly, we exploited: 1) the UPD of copper on the substrate iso-oriented polycrystalline surfaces and 2) the SLRR between palladium and copper. An H_2SO_4 0.1M + $CuSO_4$ 1mM solution was used as electrolyte for the Cu UPD step. The copper adlayer (1 ML) was obtained by applying 0.05V at the WE for two minutes. After this step, SLRR was performed by substituting the electrolyte with an $HClO_4$ 0.1M + PdCl 0.1mM solution for five minutes. Cu UPD was chosen due to the extended literature present on its use as sacrificial metal for the galvanic exchange. Moreover, Cu UPD process was also useful as a benchmark to assess the quality of the surface atomic orientation of the obtained gold electrodes, by comparison with the cyclic voltammetries on monocrystalline (1 1 1) Au [42,43].

2.2.2. Pd on Au from direct electrodeposition

For the direct deposition of Pd, a 0.1 mM $PdSO_4$ + 0.1 M H_2SO_4 solution was used. Here we performed a galvanostatic deposition using a current of 10 mA/cm2 until the total charge of approx. 10 monolayers (MLs, 1 full pseudo-morphic Pd monolayer on Au (111) = 445 C/cm2) was counted.[44]

2.2.3. Pd film from PVD

The PVD deposition of Pd was performed on one of the previously prepared gold electrodes carefully masked by paper tape on the glass side (Figure 1) using a KORVUS PVD machine equipped with a quartz crystal microbalance. The balance was calibrated just before the deposition by acquiring the balance correction factor. This absolute value was calculated by comparison between the nominal thickness of a thin Pd deposition, and its real value, obtained by FIB/SEM cross-sectioning methods [45].

2.2.4. EPMA characterization

Samples were analyzed using a JEOL-JXA 8230-EMPA device at the joint laboratory LaMA (Earth Science Department, University of Florence – CNR-IGG). The analytical conditions were 15 kV of accelerating voltage with 20 nA of beam current. The counting time was 40 s for Au and Pd. The primary standards used for calibration were Au and Pd pure metals, provided by Astimex Ltd. To determine the actual Pd loading in the samples we processed microanalysis data with the software Badger Film. [46]

2.3. GI-FEXRAV experiment

2.3.1. XAS Experiment and Beamline

XAS experiments are usually performed by impinging X-Rays at an angle between 45° and 90° with respect to the surface of the material we want to investigate. The 90° set-up is used when the absorber in the sample is concentrated (high interaction volume), and we are able to acquire the transmission signal.

The 45° geometry is used to acquire the fluorescence signal with a detector placed at 90° with respect to the beam direction. This is typically useful when the absorber is diluted or simply when the sample is too thick to allow the passage of the beam.

In the study of metal nanoparticles in a carbonaceous matrix, just like for the Pd/C catalyst used in our previous experiments [24–26], we are going to obtain a XAS signal (in both fluorescence and transmission) strongly determined by the electrochemically inert bulk of the metallic nanoparticles, to an extent higher the bigger the NPs dimensions are. To overcome this limitation, we could in principle decrease the dimension of the particles, to the point in which all the atoms of the single particles participate to the surface reactivity. Pushing this concept to the limit, we could imagine a

surface where the atoms constituting the catalyst layer are disposed forming one monolayer (ML) or less. This new catalyst leads to new spectroscopic challenges. In order to maximize the electrocatalyst sampled volume (Figure 2) we can adopt the Grazing Incidence X-ray Absorption Fine Structure (GIXAFS) experimental geometry, which exploits very low incidence angles (< 0.5°).

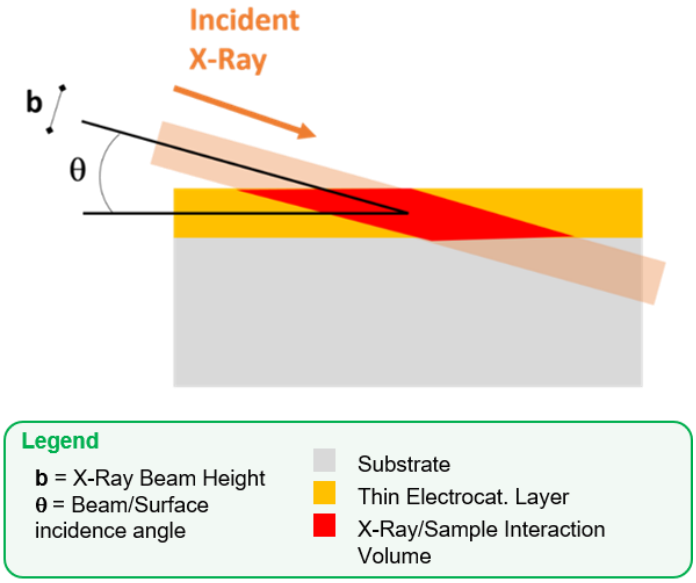

Figure 2 – Side (X-Y plane) section view of X-Ray/Thin layer sample interaction during a Grazing Incidence XAS experiment. For thin layers, an increase in interaction volume can be obtained with the decrease in the incidence angle between surface and beam

Here the GIXAFS data at the Pd K-edge (E = 24350 eV) were collected at the LISA beamline [47] operative at the European Synchrotron Radiation Facility (ESRF) in Grenoble (France) on a dedicated experimental station [48] in the course of two different experiments (MA-3431 and CH-6101) prior and after the ESRF Extremely Brilliant Source (EBS) and BM-08 beam upgrades [49]. For the first experiment (MA-3431), samples were measured after the first part of the BM08 refurbishment [50] using a pair of flat Si (111) monochromator crystals. For both MA-3173 and MA-3431 a pair of Pt-coated cylindrical mirrors (E cutoff ≃ 40 keV) was used for harmonic rejection and for the vertical focus on the sample (beam size ~2000 (H) µm x 150 (V) µm). Experiment CH-6101 was performed after the ESRF upgrade to EBS; samples were measured with the complete BM08 setup [50], using a pair of flat Si (311) monochromator crystals and Pt coated toroidal focusing mirrors (Ecutoff ≈ 40 KeV), beam size was ~150 (H) µm x 150 (V) µm.
The incident and reflected beams have been collected by two ion chambers, and a preliminary spectrum without the sample was used to scale the reflected intensity to absolute reflectivity values. A Ge multielement detector, placed on the side of the cell, at 90° with respect to the X-ray optical pathway, was used to collect the fluorescence signal. For each sample, the angles were selected for the GIXAFS data collection, in order to maintain them higher in respect to the critical angle for total reflection (incident beam angle < 0.5°). In fact, due to a slightly uneven distribution of the deposit on the glass slide caused by the sputterer geometry, we were not able to work in total reflection mode (reflEXAFS). [51,52]

2.3.2. The Electrochemical Cell

The cell used for the experiment was designed to enable the particular experimental conditions required during simultaneous electrochemistry and XAS on thin film. It was machined out from a bar of polymethyl methacrylate (PMMA) at the INFN workshop of Sesto Fiorentino (Florence).

The following constructive criteria were considered during cell design:

a) the catalytical surface had to be placed face up on the bottom of the electrochemical cell;

b) an extended electrode surface had to be exposed inside the solution, in order to permit the lower possible angle for the grazing incidence measurements, and to sample a bigger number of Pd atoms;

c) cell walls towards fluorescence detector had to be as thin as possible to minimize X-ray dampening;

d) an electrical contact has to be maintained between the outer and the inner part of the EC-cell without the introduction of electrochemically unstable metals in contact with the solution;

e) the un-irradiated conductive film area has to be minimized, in order to decrease current during cyclic voltammetries, and thus preventing potentiostat current saturation;

f) no electrode has to be on the optical beam pathway.

In order to overcome all these issues, we adopted the design visible in Figure 3.

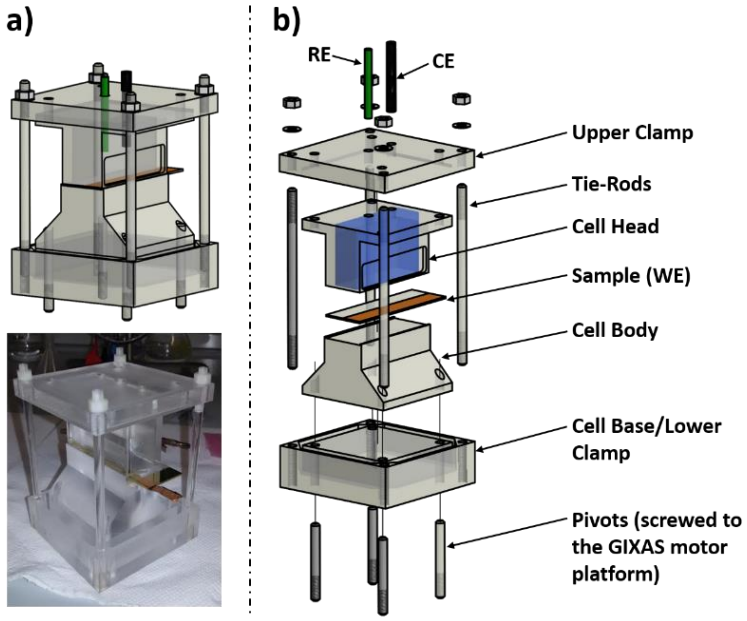

Figure 3 – Electrochemical Cell schematics: a) The rendering of the assembled cell, together with its photo, b) an exploded view of the cell, depicting its different elements

In this configuration, the Electrochemical Cell is created between the sample surface (bottom) and the cell head (which is a reversed basin). The sealing of the cell towards electrolyte spilling is granted by the high level of flatness of both the sample surface and the machined bottom side of the cell head. The head tank is designed to hold approximately 10 cm3 of the electrolytic solution. The chosen geometry permitted the use of the GIXAS technique enabling the acquisition geometry visible in Figure 4-a. Following design criteria a), b) and c) an extended portion of the sample surface was placed in contact with the solution along the X-axis, and a wall thinning on the detector side permits to minimize the dampening of the output fluorescence intensity (Figure 4). In agreement with criterion d), the electrical contact with the potentiostat was granted by the continuous Au film which extends in the back of the cell (Figure 4, X-Y Section).

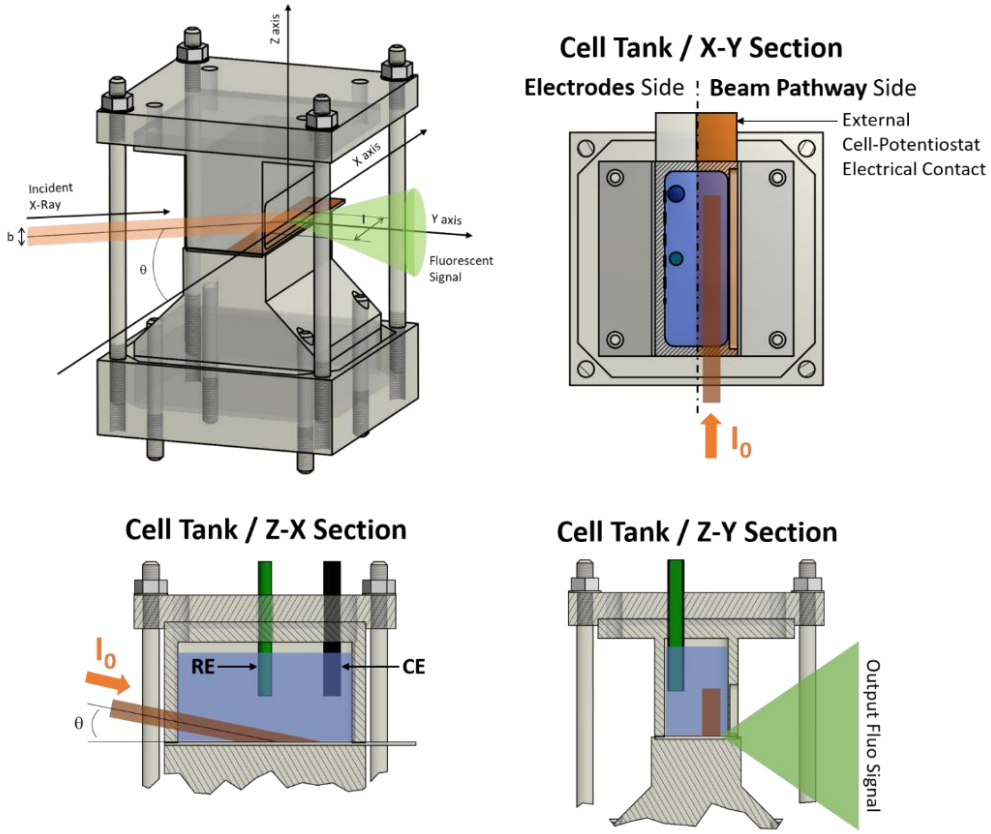

Figure 4 – Various Cell views depicting its working principle

3. RESULTS AND DISCUSSION

3.1. Polycrystalline isoriented Au (111) substrate characterization

The substrates were prepared in different batches exploiting three different heat treatment methods, A pool of un-annealed samples was used for comparison. The labelling of the samples, together with their description can be found in Table 1.

Label	Sample
a)	Un-annealed
b)	Flame-annealed
c)	Oven-annealed 3h
d)	Oven-annealed 6h

Table 1 – Label/Type correlation for the heat-treated samples

After the different heat treatments, no naked-eye change was noticeable among the samples. A SEM characterization was performed to assess variations at the micro-to-nano level in the surface morphology (Figure 5), showing a strong influence of the preparation method on the surfaces in the small scale. Un-annealed samples (Figure 5-a) showed a bumpy structure, typical of a fast 3D grain growth, while the flame-annealing (Figure 5-b) lead to smoother surfaces, contemporary highlighting the trenches between the deposit islands (as seen in the untreated samples). For the Oven-annealed samples (Figure 5-c and -d), further increase in substrate homogeneity with the increase in process time (from 3 to 6 hours) was noticeable, with the loss of the gaps, and a strong smoothening of the surfaces. An interesting fact to notice was the average increase on the voids (holes), which arise again for the 6 hours Oven-annealed samples with respect to the 3 hours Oven-annealed samples. Concluding, SEM showed a progressive smoothing of the gold surface which followed the trend Un-annealed < Flame-annealed < Oven-annealed 3h < Oven-annealed 6h.

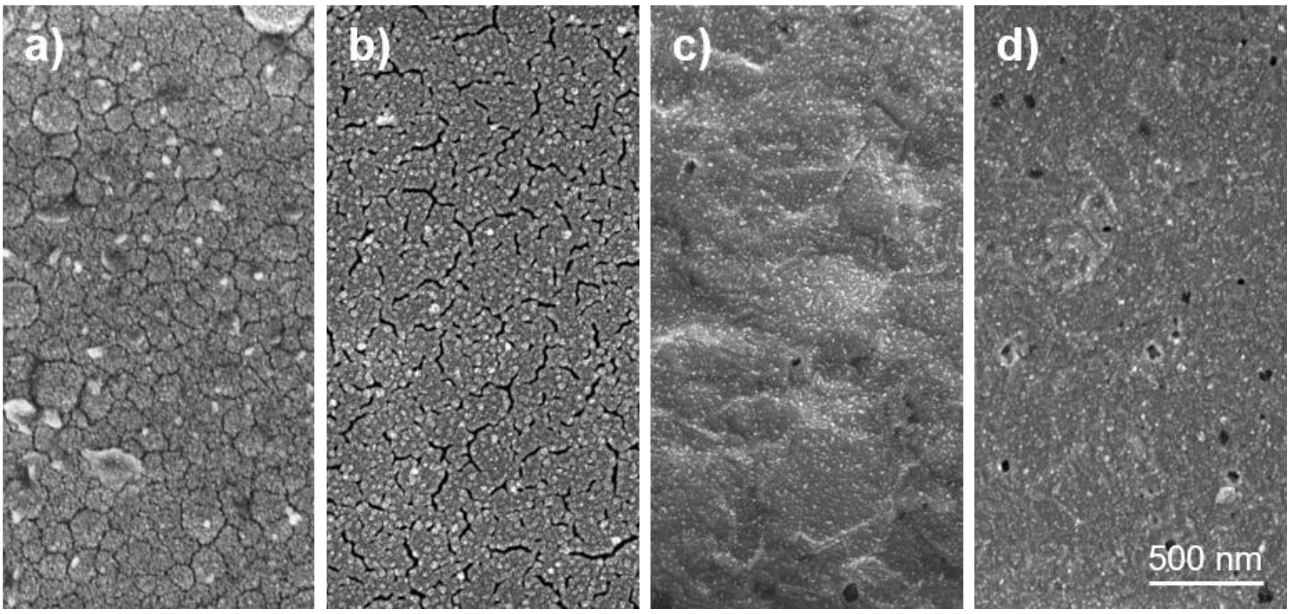

Figure 5 – SEM of the sample surfaces after: a) un-annealed, b) Flame-annealing, c) Oven-annealing for 3 hours and d) Oven-annealing for 6 hours.

To further quantify the degree of smoothness of the surfaces, AFM characterization (Figure S1) was used to extract sample roughness. The trend seen during SEM characterization was confirmed from the data acquired from the rasterings, as visible in Table 2.

	a)	**b)**	**c)**	**d)**
R_a [nm]	3.7 ± 0.5	2.9 ± 0.2	2.6 ± 0.7	2.4 ± 0.3
R_q [nm]	4.9 ± 0.3	3.6 ± 0.3	3.3 ± 1	3.0 ± 0.4
R_t [nm]	30 ± 2	20 ± 2	22 ± 8	17 ± 1
R_{tm} [nm]	23 ± 2	16 ± 2	15 ± 4	12.7 ± 0.6

Table 2 – Roughness parameters for the samples: a) Un-annealed, b) Flame-annealed, c) Oven-annealed 3 hours and d) Oven-annealed 6 hours, where R_a is the arithmetic average height, R_q the root mean square roughness, R_t the maximum height of the profile and R_{tm} the mean of maximum peak-to-valley height

Finally, to assess the degree of atomic order of the Au surfaces, we tested the different batches of annealed and un-annealed samples towards the copper UPD. It is known that polycrystalline gold surfaces, when subjected to temperatures above 500°C, tend to rearrange following a herringbone pattern, iso-orienting each single grain surface by the Au (111) structure [39,53]. This gold property is particularly important, as it permits to create ordered structures, which can be used effectively for surface limited electrochemical reactions. Amidst them, the Under Potential Deposition (UPD) phenomenon can be effectively achieved [54–56]. Among the different UPDs that can be used, Copper shows two different deposition peaks, related to two different Cu coverages on the surface: The 0.6 monolayer (ML) coverage starting at 0.25 V, and a 1 ML coverage occurring at 0.10 V vs. Ag/AgCl/KCl sat. (Equivalent respectively to approx. 0.35 V approximately [57,58]. Being part of the UPD + SLRR process, Copper deposition is also a good benchmark of the order reached by surface Au atoms after the gold heat treatments. In Figure 6 the cyclic voltammetries produced using the gold surface as working electrodes at a scan speed of 50 mV/s are reported. An important change in the peaks definition was visible between the un-annealed samples CVs (black) and the heat-treated ones, both for the flame-annealed and the oven-annealed, whit a good resemblance between Flame-Annealed and 6h Oven Annealed CVs, the traces of which almost overlap in the Cu UPD potential region (around 0.00 V vs Ag/AgCl/KCl sat.).
Surprisingly, our gold surfaces showed only a small broadening of the cathodic UPD peaks related to the deposition of 0.6 ML and 1.0 ML of copper on surface.

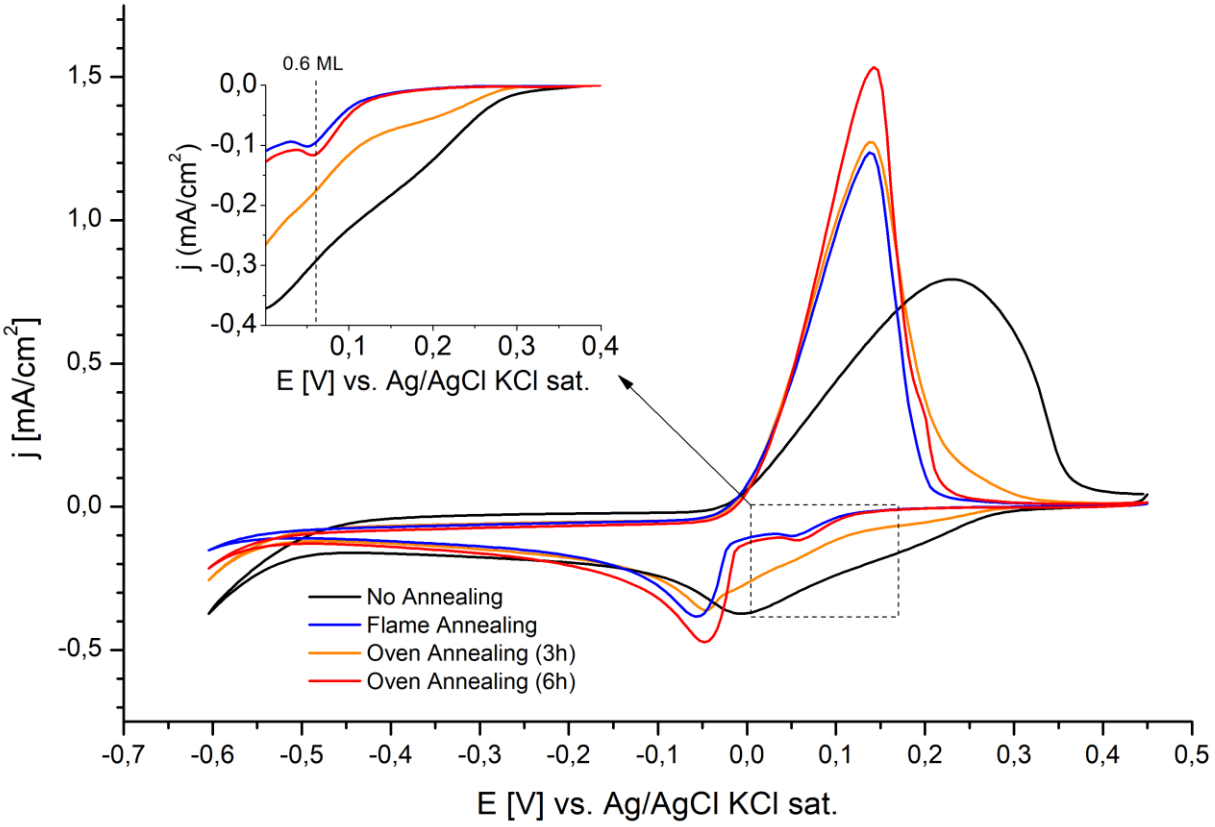

Figure 6 – Cyclic voltammetries of the electrodes in a H_2SO_4 0.1M + $CuSO_4$ 1 mM solution showing the typical UPD peaks

3.2. Characterization of the Pd-Au electrodes at different loading for GI-FEXRAV tests

Once deposited on the polycrystalline Au electrode, the palladium layers, prepared following the procedures described in 2.2., were characterized both electrochemically, and by the use of EPMA, in order to assess the coverage and the distribution of the film. The electrochemical characterization was performed using the Au-Pd surfaces as working electrodes inside the GI-FEXRAV cell, in an NaOH 1M + EtOH 1M electrolyte, in order to track and compare the typical Gold and Palladium voltammetric curves toward ethanol electro-oxidation. Results reported in Figure 7 showed an interestingly precise trend among the samples. For the bare gold substrate (Figure 7-a), the typical Ethanol oxidation peaks on Au (Au forward or Au_f = 1.22 V vs. RHE and Au backward or Au_b = 1.05 V vs. RHE) [59] were clearly visible for both the scan directions, with a peak current on the forward scan of about 14 mA/cm2. For the surface-controlled Pd sub-mono layer deposition on Au (Figure 7-b), the two series of peaks coming from the oxidation of EtOH on Palladium (Pd forward or Pd_f = 0.81 V vs. RHE and Pd backward or Pd_b = 0.67 V vs. RHE)[59,60] and on Gold were clearly separated and visible, demonstrating the presence of two distinct surfaces acting differently in contact with the electrolytic solution, and thus no alloying or synergistic effect. Same double-surface behavior was visible for the electrode produced by direct electrodeposition of Pd (Figure 7-c). This time, the decrease in the Au peak currents was in line with an increase of Pd coverage, which in turn seemed to be less active in respect to the surface-limited deposit. We reached complete Pd coverage only for the Pd PVD deposition (Figure 7-d), where it was possible to notice the disappearance of the typical Au peaks.

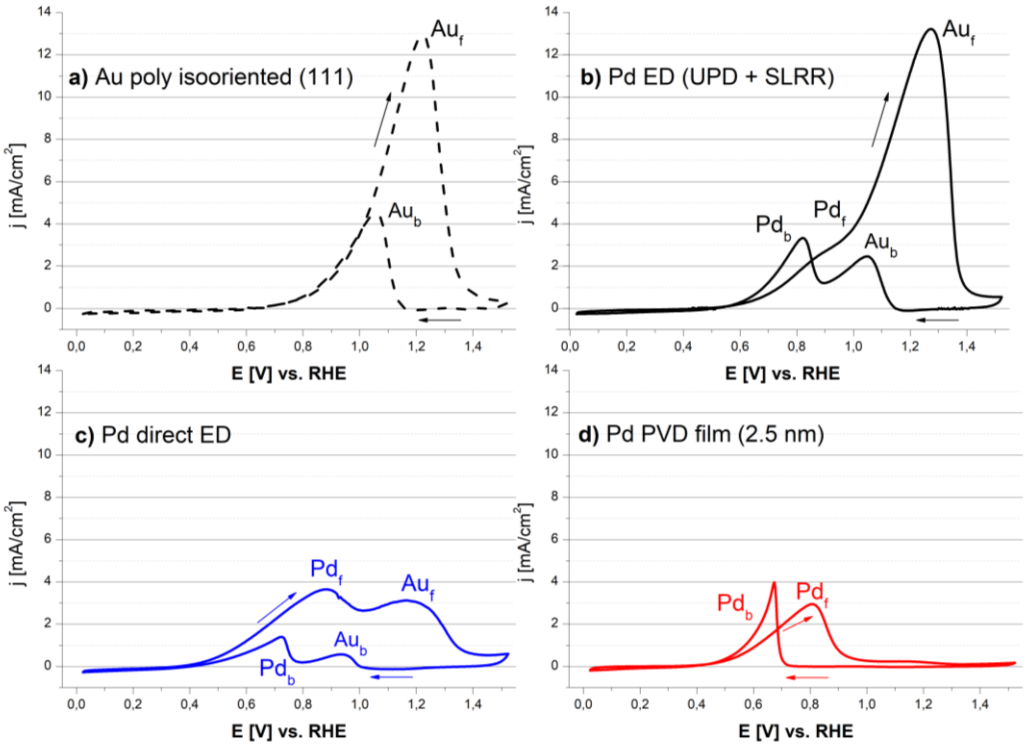

Figure 7 – Comparison between Electrochemical responses in NaOH 1M + EtOH 1M from the different Pd-Au electrodes, scan speed 50 mV/sec

Interestingly, the uncompleted coverage Pd deposit (UPD + SLRR) showed doubled max current densities in respect to the direct electrodeposition and to the PVD deposition, suggesting a far bigger electroactive area of the former with a lower metal loading in respect to the latter two cases with higher Pd content. The UPD+SLRR < Direct ED < PVD loading trend was confirmed also by EPMA characterization, used to deduce an average Pd loading of the surfaces. Specifically, a loading of 2.2 μg/cm^2 was extrapolated for the ultra-low Pd loading (UPD+SLRR), while for the Direct Pd Electrodeposition and for the PVD electrodeposition processes, values of 5.6 μg/cm^2 and 8.4 μg/cm^2 were obtained respectively. EPMA was used instead of XRF [61–63] because of the lower degree of permeation of electrons in the bulk of the material in respect to x-rays, and consequently the higher sensitivity in respect to surface composition.

3.3. XAS experiment

GI-FEXRAV technique was tested on the three different Palladium-loaded Au electrodes. The use of different loadings of Pd on the Au base electrodes gave us a chance to better describe the method and its present-stage limitations. The sample prepared by UPD+SLRR, due to its ultra-low Pd loading, was useful to test the lower detecting capability of the technique; as reported in paragraph 3.2, EPMA found the smallest Palladium loading on this Au surface. The second sample, where the direct deposition of Pd took place, contained an intermediate loading of Pd. The third sample, the thick PVD Palladium deposit, was equivalent to a low surface to volume particle dispersion, where only a small fraction of Pd atoms (approx. 5%) participated to the surface reactivity. The samples were not tested towards GI-FEXRAV consequentially. The Intermediate Pd loading sample was examined on the BM-08 beamline prior to ESRF-EBS upgrade, while the Low and High loading samples were examined on the same line after the accelerator refurbishment. At the present stage, we were able to study Pd to PdO transition using effectively the GI-FEXRAV technique on the intermediate loading sample only, by following its oxidation back and forth, just like we performed before using powdered Pd/C catalysts [25]. An unsuccessful attempt on the low loading sample was made during the first experiment (MA-3431) in order to acquire the in-situ spectra (sub-monolayer). The same in-situ spectra were easily obtainable after ESRF-EBS upgrade, during EXP CH-6101. Sadly, during this second turn, we had not enough time in order to perfect the beamline set-up for a GI-FEXRAV data collection of the low Pd loading.

3.3.1. Ultra-low loadings of Pd on Au from electrochemical UPD+SLRR

We probed the Pd on the UPD + SLRR sample using Grazing Incidence XAS, ex-situ, in-situ and in-operando. The

ex-situ acquisition was first performed to acquire the initial situation of the Pd ultra-thin film. The acquired fluorescence spectra (Figure 8) was compared with Pd and a PdO standard spectra using a linear combination fit technique, in order to esteem the initial ratio between the two species, representing the absolute majority of the species present on the surface in standard conditions. [24] The films resulted consisting by almost 2/3 of metallic Pd (63%), and by 1/3 of PdO (37%). We tested the same electrode during an operando XAS, by assembling the EC cell in NaOH 2M and acquiring XANES spectra after static potential tests (30 minutes hold) at increasingly higher potentials (0.05 V, 0.50 V and 1.00 V vs. RHE). We were still able to acquire the edge jump of the Pd (Figure 9) and, despite the noisy nature of these spectra, to notice the increase in intensity of the PdO peak (at about 24370 eV) from the 0.05 V vs. RHE potential step to the 0.50 V vs. RHE. No particular change in the near edge fingerprint was noticed between 0.50 V vs. RHE and 1.00 V vs. RHE. Here, despite the increase in the PdO-related peak, we were still able to see the peak just before 24400 eV, related to the presence of metallic Pd on the surface. This initial evidence, together with the results obtained from the electrochemistry (Figure 7) suggested the presence of portions of sample with un-oxidized palladium, and hence the formation of 3D islands of Pd atoms during the SLRR, instead of a flat homogeneous sub-monolayer. We finally tested the system in-operando, using the GI-FEXRAV technique during our last experiment (EXP CH-6101), by fixing the beam energy at 24370 eV and by performing voltammetries with a scan speed of 1 mV/sec. We were not able to dedicate sufficient time for the optimization of the acquisition parameters (like the integration time for the fluorescence signal, which was approx. 1 second, in line with the voltammetric scan speed, much lower in respect to the one used for direct electrodeposition which was approximately 2 seconds), ultimately not being able to acquire a discrete fixed energy absorption signal variation above the detector noise in the timespan of the experiment.

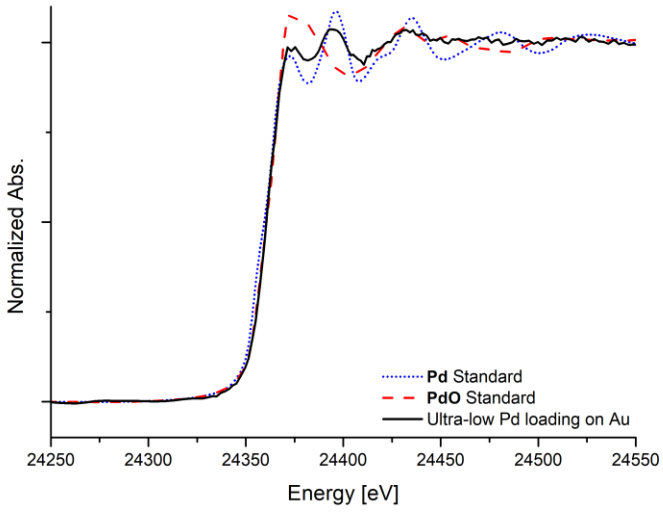

Figure 8 – Ex-Situ XANES of the Ultra-thin layer of Pd from UPD+SLRR

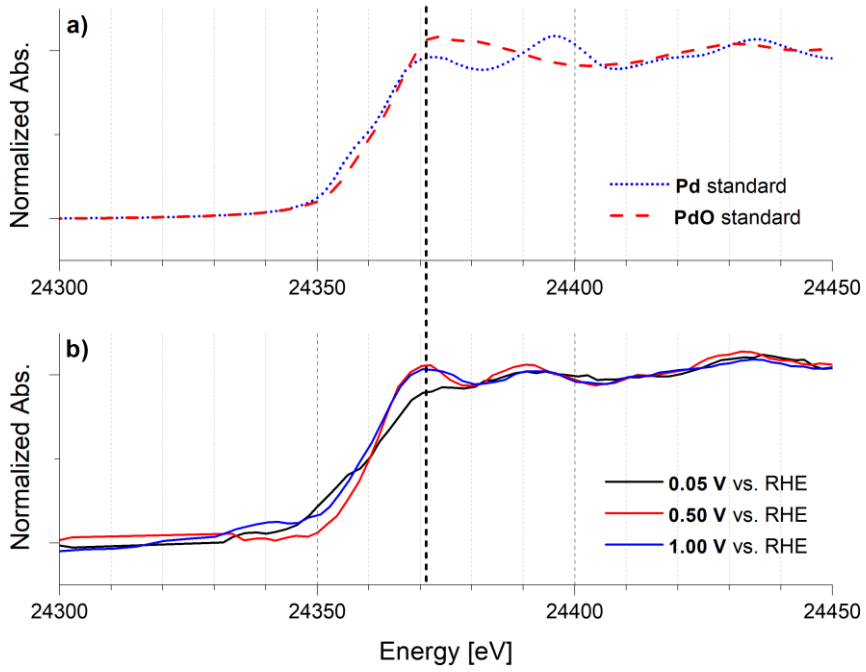

Figure 9 – in-situ XANES of the Ultra-thin layer of Pd from UPD+SLRR, performed after a 30 minutes steps at fixed potentials of: 0.05 V vs. RHE (Black), 0.50 V vs. RHE (Red) and 1.00 V vs. RHE (Blue). Potential was kept active during the whole acquisition

3.3.2. Direct Pd Electrodeposition

For the electrodeposited Palladium films loading, we tested directly the GI-FEXRAV technique using a beam energy of 24370 eV and by performing voltammetries with a scan speed of 0.5 mV/sec, from 0.20 V to 1.20 V vs RHE, and an integration time for the fluorescent signal of 2 seconds. With this set-up, we managed to acquire variations of the absorption signal with the potential, as visible in Figure 10 , with a well-defined voltammetry, which mimicked the one of the oxidation of a bulk palladium polycrystalline surface.

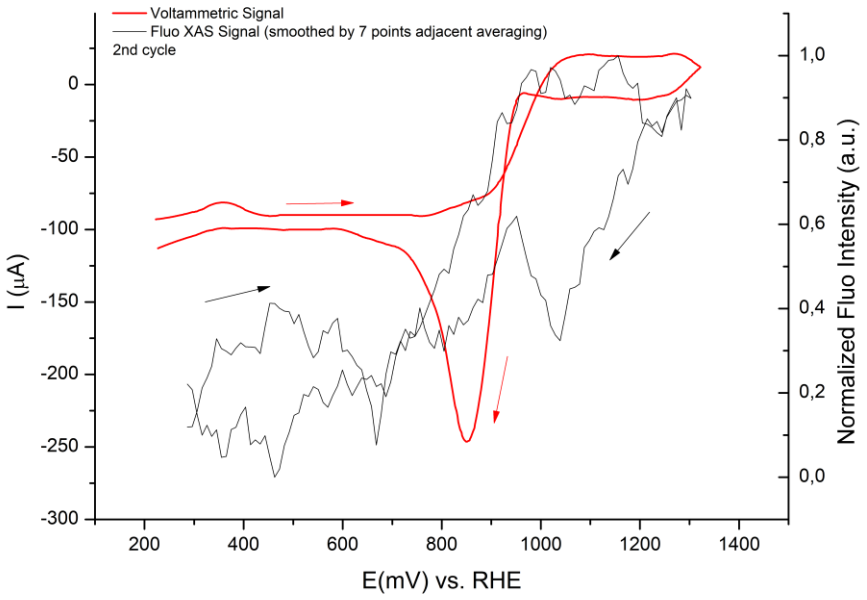

Figure 10 – 2nd GI-FEXRAV scan on the surface of the directly electrodeposited Pd (Vscan 0.5 mV/s)

Moreover, by analysing the trend of the absorption signal with the voltametric scan progression (Figure 11) we were able to notice the same decrease in the overall signal which was visible for the Pd/C system in our previous experiments

in the bare alkaline electrolyte. [24,64,65]

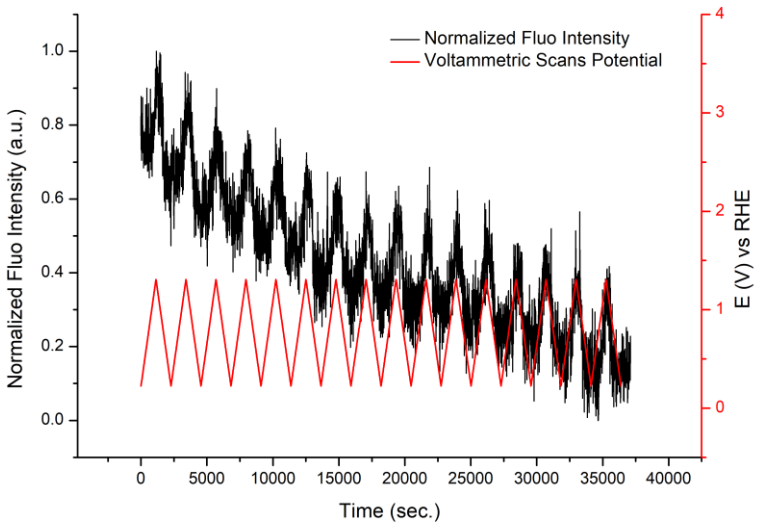

Figure 11 – An image reporting all the GI-FEXRAV cycles, showing the overall decrease in the fluorescence absorption signal due to Pd dissolution at the electrode.

3.3.3.PVD Pd deposition

A third series of XAS acquisitions was performed on the PVD-deposited Palladium thin layers. Tests were similar to the in-situ performed on the previous ultra-low loaded Pd sample, in which we acquired the XANES spectra of the surface after 30 minutes at increasingly higher potential. This time we tested an additional step in potential between 0.50 V and 1.00 V, forcing the electrode under oxidative stress for a longer overall time interval. Then, after the 1.00 V step, we acquired a spectrum after 30 minutes at Open Circuit Potential, and another one after half an hour at 0.05 V.

By first analysis, spectra from all the potential steps seemed similar, with a fingerprint typical of metallic Pd (Figure 12-a). A small coherent change in composition was noticeable only after the linear combination fit, using Pd and PdO standards as extremes for the fitting. From this elaboration, a small decrease in the amount of metallic Pd was noticeable from the 0.05 V scan (approx. 67.5%) to the 1.00 V scan (62%). Obviously, the Pd(II) followed the opposite trend, from 32.5% of the 0.05 V scan to the 38% of the 1.00 V scan. Interestingly, OCP after the 1.00V lead to no change of the Pd(0)/Pd(II) ratio, while the subsequent step at 0.05V moved the speciation to values similar to the initial ones (1). This trend suggested the growth of a homogeneous and thick PdO from the surface of the bulk catalytical deposit, as a consequence of the increase of the WE applied potential. The reaction seemed almost reversible with the backward conversion of Pd(II) to Pd(0) to the initial ratios (1) when the potential was switched back from 1.00 V to 0.05 V. The overall oxide thickness remained however much smaller in respect to the metallic palladium width, not allowing the adoption of the GI-FEXRAV technique for this system.

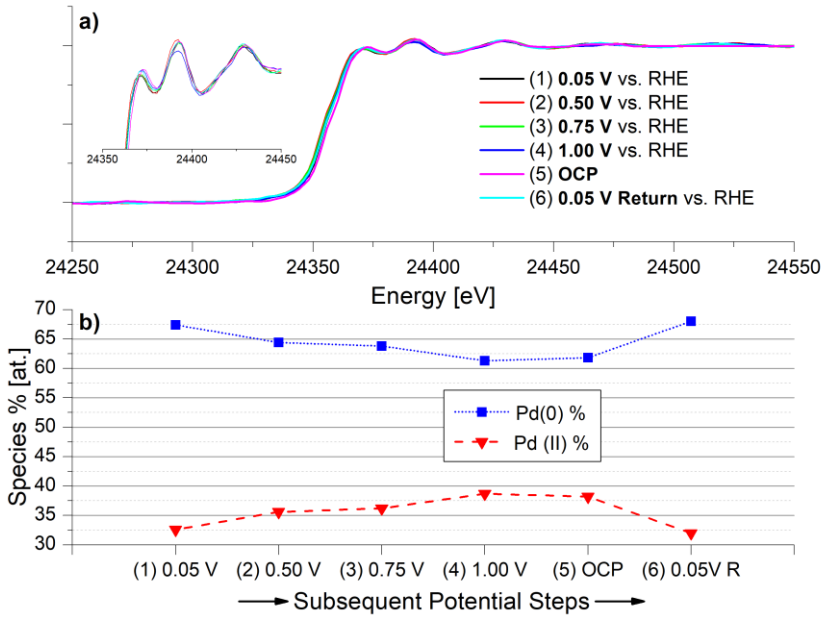

Figure 12 – XAS experiment on the PVD deposited sample: a) XANES spectra in grazing incidence at different potential steps and b) Pd and PdO species variation between consecutive potential steps

4. CONCLUSION

In this article, we present a robust, cheap and versatile procedure to produce wide, structurally oriented and cheap Au electrodes that can be used as base platforms for fundamental studies in electrocatalysis. These electrodes were used to grow ultra-thin Pd model surfaces, which mimicked the electrochemical behavior of polycrystalline Palladium for the Ethanol Oxidation Reaction. Specifically, these deposits were growth on the Au surfaces exploiting three different methods: 1) Surface Limited Electrodeposition (lower loadings composed by sub-monolayered Pd), 2) Direct Electrodeposition and 3) PVD Pd deposition (thick deposit). This particular electrode design was guided by the will to use the electrocatalytical surfaces for operando grazing incidence XAS, which is also presented in the article. Particularly, a new experimental design was developed (Grazing Incidence FEXRAV, or GI-FEXRAV) and used to follow the Palladium surfaces evolution during electrochemical stimulus in alkaline electrolyte. Until now, we were able to follow the speciation of Pd using GI-FEXRAV for a thin Pd film obtained by direct electrodeposition, where the amount of Pd was still low enough not to cover the whole gold electrodic surface. We explored the capability of the XAS technique also for thicker palladium films prepared using PVD methods. Here we were not able to use GI-FEXRAV due to the intrinsically low surface-to-volume ratio of the deposits, with the bulk absorption signal overshadowing the signal of the surface atoms, the ones participating to the red/ox reaction. Finally, the test performed on the sub-monolayered Palladium deposit, produced by surface-limited deposition, permitted us to detect chemical transformations of Pd in-situ. Still, we were not able to optimize the acquisition for the Grazing Incidence XAS during the last experiment, which will surely be done in the next experimental runs. In conclusion, the GI-FEXRAV has been used successfully to characterize *in-operando* and *in-situ* Pd(0)/Pd(II) ultra-low loading systems, with results in line with the ones seen during our previous experiments on Pd/C powdery electrocatalysts, but with a more precise electrochemical response, and a much lower palladium loading. GI-FEXRAV application, together with the use of the presented wide, cheap and robust electroactive Au surfaces, could possibly represent an important tool for future electrocatalyst study and understanding. Future work by our group will be aimed to improve the efficacy of the GI-FEXRAV technique with the latest, more performing beamline set-up. The improvement in beamline control will surely enable us for the characterization of very low amount of metal, like the ones present on the sub-monolayer substrates.

5. ACKNOWLEDGMENTS & FUNDING

Authors wanted to thank PRIN 2017 Project “Novel Multilayered and Micro-Machined Electrode Nano-Architectures for Electrocatalytic Applications (Fuel Cells and Electrolyzers)” (N° 2017YH9MRK) funded by Italian Ministry MUIR. Authors wanted to acknowledge the European Synchrotron Radiation Facility (ESRF) for provision of synchrotron radiation facilities for EXP MA-3431 and CH-6101.

6. BIBLIOGRAPHY

[1] Y. Yun, Alcohol Fuels: Current Status and Future Direction, in: Alcohol Fuels - Current Technologies and Future Prospect, IntechOpen, 2020. https://doi.org/10.5772/intechopen.89788.

[2] Direct Alcohol Fuel Cells for Portable Applications, Elsevier, 2018. https://doi.org/10.1016/C2016-0-00632-0.

[3] Y. Chen, M. Bellini, M. Bevilacqua, P. Fornasiero, A. Lavacchi, H.A. Miller, L. Wang, F. Vizza, Direct Alcohol Fuel Cells: Toward the Power Densities of Hydrogen-Fed Proton Exchange Membrane Fuel Cells, ChemSusChem. 8 (2015) 524–533. https://doi.org/10.1002/cssc.201402999.

[4] M.A. Damin Zhanga, Jia Dua, Jonathan Quinsonb, On the electro-oxidation of small organic molecules: towards a fuel cell catalyst testing platform with realistic reaction environment Damin Zhang, ChemXiv. (n.d.) 1–24.

[5] E. Berretti, L. Osmieri, V. Baglio, H.A. Miller, J. Filippi, F. Vizza, M. Santamaria, S. Specchia, C. Santoro, A. Lavacchi, Direct Alcohol Fuel Cells: A Comparative Review of Acidic and Alkaline Systems, Electrochemical Energy Reviews. 6 (2023) 30. https://doi.org/10.1007/s41918-023-00189-3.

[6] Y.X. Chen, A. Lavacchi, H.A. Miller, M. Bevilacqua, J. Filippi, M. Innocenti, A. Marchionni, W. Oberhauser, L. Wang, F. Vizza, Nanotechnology makes biomass electrolysis more energy efficient than water electrolysis, Nat Commun. 5 (2014) 4036. https://doi.org/10.1038/ncomms5036.

[7] H.A. Miller, A. Lavacchi, F. Vizza, Storage of renewable energy in fuels and chemicals through electrochemical reforming of bioalcohols, Curr Opin Electrochem. 21 (2020) 140–145. https://doi.org/10.1016/j.coelec.2020.02.001.

[8] A. Lavacchi, H. Miller, F. Vizza, Nanotechnology in Electrocatalysis for Energy, Springer New York, New York, NY, 2013. https://doi.org/10.1007/978-1-4899-8059-5.

[9] European Commission, Study on the Critical Raw Materials for the EU 2023 – Final Report, n.d. https://data.europa.eu/doi/10.2873/725585 (accessed October 9, 2023).

[10] H. Kim, T.Y. Yoo, M.S. Bootharaju, J.H. Kim, D.Y. Chung, T. Hyeon, Noble Metal-Based Multimetallic Nanoparticles for Electrocatalytic Applications, Advanced Science. 9 (2022) 2104054. https://doi.org/10.1002/advs.202104054.

[11] Y. Chen, M. Bellini, M. Bevilacqua, P. Fornasiero, A. Lavacchi, H.A. Miller, L. Wang, F. Vizza, Direct Alcohol Fuel Cells: Toward the Power Densities of Hydrogen-Fed Proton Exchange Membrane Fuel Cells, ChemSusChem. 8 (2015) 524–533. https://doi.org/10.1002/cssc.201402999.

[12] V. Bambagioni, C. Bianchini, Y. Chen, J. Filippi, P. Fornasiero, M. Innocenti, A. Lavacchi, A. Marchionni, W. Oberhauser, F. Vizza, Energy Efficiency Enhancement of Ethanol Electrooxidation on Pd–CeO 2 /C in Passive and Active Polymer Electrolyte-Membrane Fuel Cells, ChemSusChem. 5 (2012) 1266–1273. https://doi.org/10.1002/cssc.201100738.

[13] H.A. Miller, A. Lavacchi, F. Vizza, M. Marelli, F. Di Benedetto, F. D'Acapito, Y. Paska, M. Page, D.R. Dekel, A Pd/C-CeO 2 Anode Catalyst for High-Performance Platinum-Free Anion Exchange Membrane Fuel Cells, Angewandte Chemie International Edition. 55 (2016) 6004–6007. https://doi.org/10.1002/anie.201600647.

[14] E. Berretti, M. Longhi, P. Atanassov, D. Sebastián, C. lo Vecchio, V. Baglio, A. Serov, A. Marchionni, F. Vizza, C. Santoro, A. Lavacchi, Platinum group metal-free Fe-based (Fe N C) oxygen reduction electrocatalysts for direct alcohol fuel cells, Curr Opin Electrochem. 29 (2021) 100756. https://doi.org/10.1016/j.coelec.2021.100756.

[15] S.A. Mirshokraee, M. Muhyuddin, R. Morina, L. Poggini, E. Berretti, M. Bellini, A. Lavacchi, C. Ferrara, C. Santoro, Upcycling of waste lithium-cobalt-oxide from spent batteries into electrocatalysts for hydrogen evolution reaction and oxygen reduction reaction: A strategy to turn the trash into treasure, J Power Sources. 557 (2023) 232571. https://doi.org/10.1016/j.jpowsour.2022.232571.

[16] S.A. Mirshokraee, M. Muhyuddin, R. Lorenzi, G. Tseberlidis, C. Lo Vecchio, V. Baglio, E. Berretti, A. Lavacchi, C. Santoro, Litchi-derived platinum group metal-free electrocatalysts for oxygen reduction reaction and hydrogen evolution reaction in alkaline media, SusMat. 3 (2023) 248–262. https://doi.org/10.1002/sus2.121.

[17] M. Muhyuddin, A. Friedman, F. Poli, E. Petri, H. Honig, F. Basile, A. Fasolini, R. Lorenzi, E. Berretti, M. Bellini, A. Lavacchi, L. Elbaz, C. Santoro, F. Soavi, Lignin-derived bimetallic platinum group metal-free oxygen reduction reaction electrocatalysts for acid and alkaline fuel cells, J Power Sources. 556 (2023) 232416. https://doi.org/10.1016/j.jpowsour.2022.232416.

[18] D. Testa, G. Zuccante, M. Muhyuddin, R. Landone, A. Scommegna, R. Lorenzi, M. Acciarri, E. Petri, F. Soavi, L. Poggini, L. Capozzoli, A. Lavacchi, N. Lamanna, A. Franzetti, L. Zoia, C. Santoro, Giving New Life to Waste Cigarette Butts: Transformation into Platinum Group Metal-Free Electrocatalysts for Oxygen Reduction Reaction in Acid, Neutral and Alkaline Environment, Catalysts. 13 (2023) 635. https://doi.org/10.3390/catal13030635.

[19] S.A. Mirshokraee, M. Muhyuddin, J. Orsilli, E. Berretti, L. Capozzoli, A. Lavacchi, C. Lo Vecchio, V. Baglio, A. Galli, A. Zaffora, F. Di Franco, M. Santamaria, L. Olivi, S. Pollastri, C. Santoro, Mono-, bi- and tri-metallic platinum group metal-free electrocatalyst for hydrogen evolution reaction following a facile synthetic route, Industrial Chemistry & Materials. (2023). https://doi.org/10.1039/D3IM00058C.

[20] M. Fracchia, P. Ghigna, A. Vertova, S. Rondinini, A. Minguzzi, Time-Resolved X-ray Absorption Spectroscopy in (Photo)Electrochemistry, Surfaces. 1 (2018) 138–150. https://doi.org/10.3390/surfaces1010011.

[21] A. Minguzzi, O. Lugaresi, C. Locatelli, S. Rondinini, F. D'Acapito, E. Achilli, P. Ghigna, Fixed energy X-ray absorption voltammetry, Anal Chem. 85 (2013) 7009–7013. https://doi.org/10.1021/ac401414v.

[22] M. Fracchia, A. Visibile, E. Ahlberg, A. Vertova, A. Minguzzi, P. Ghigna, S. Rondinini, α- and γ-FeOOH: Stability, Reversibility, and Nature of the Active Phase under Hydrogen Evolution, ACS Appl Energy Mater. 1 (2018) 1716–1725. https://doi.org/10.1021/acsaem.8b00209.

[23] S. Rondinini, O. Lugaresi, E. Achilli, C. Locatelli, A. Minguzzi, A. Vertova, P. Ghigna, C. Comninellis, Fixed Energy X-ray Absorption Voltammetry and Extended X-ray Absorption fine Structure of Ag nanoparticle electrodes, Journal of Electroanalytical Chemistry. 766 (2016) 71–77. https://doi.org/10.1016/j.jelechem.2016.01.039.

[24] G. Montegrossi, A. Giaccherini, E. Berretti, F. Di Benedetto, M. Innocenti, F. D'Acapito, A. Lavacchi, F. Di Benedetto, M. Innocenti, F. D'Acapito, A. Lavacchi, F. Di Benedetto, M.

Innocenti, F. D'Acapito, A. Lavacchi, Computational Speciation Models: A Tool for the Interpretation of Spectroelectrochemistry for Catalytic Layers under Operative Conditions, J Electrochem Soc. 164 (2017) E3690–E3695. https://doi.org/10.1149/2.0711711jes.

[25] Berretti, Giaccherini, Montegrossi, D'Acapito, di Benedetto, Zafferoni, Puri, Lepore, Miller, Giurlani, Innocenti, Vizza, Lavacchi, In-situ Quantification of Nanoparticles Oxidation: A Fixed Energy X-ray Absorption Approach, Catalysts. 9 (2019) 659. https://doi.org/10.3390/catal9080659.

[26] E. Berretti, M.V. Pagliaro, A. Giaccherini, G. Montegrossi, F. di Benedetto, G.O. Lepore, F. D'Acapito, F. Vizza, A. Lavacchi, Experimental evidence of palladium dissolution in anodes for alkaline direct ethanol and formate fuel cells, Electrochim Acta. 418 (2022) 140351. https://doi.org/10.1016/j.electacta.2022.140351.

[27] L. Wang, V. Bambagioni, M. Bevilacqua, C. Bianchini, J. Filippi, A. Lavacchi, A. Marchionni, F. Vizza, X. Fang, P.K. Shen, Sodium borohydride as an additive to enhance the performance of direct ethanol fuel cells, J Power Sources. 195 (2010) 8036–8043. https://doi.org/10.1016/j.jpowsour.2010.06.101.

[28] L.K. Tsui, C. Zafferoni, A. Lavacchi, M. Innocenti, F. Vizza, G. Zangari, Electrocatalytic activity and operational stability of electrodeposited Pd-Co films towards ethanol oxidation in alkaline electrolytes, J Power Sources. (2015). https://doi.org/10.1016/j.jpowsour.2015.05.121.

[29] H. Miller, J. Ruggeri, A. Marchionni, M. Bellini, M. Pagliaro, C. Bartoli, A. Pucci, E. Passaglia, F. Vizza, Improving the Energy Efficiency of Direct Formate Fuel Cells with a Pd/C-CeO2 Anode Catalyst and Anion Exchange Ionomer in the Catalyst Layer, Energies (Basel). 11 (2018) 369. https://doi.org/10.3390/en11020369.

[30] C. Bianchini, P.K. Shen, Palladium-Based Electrocatalysts for Alcohol Oxidation in Half Cells and in Direct Alcohol Fuel Cells, Chem Rev. 109 (2009) 4183–4206. https://doi.org/10.1021/cr9000995.

[31] M.V. Pagliaro, H.A. Miller, M. Bellini, B. Di Vico, W. Oberhauser, G. Zangari, M. Innocenti, F. Vizza, Electrochemical reactor for sustainable transformation of bio-mass derived allyl alcohol into acrylate and pure hydrogen, Inorganica Chim Acta. 525 (2021) 120488. https://doi.org/10.1016/j.ica.2021.120488.

[32] G.A.B. Mello, C. Busó-Rogero, E. Herrero, J.M. Feliu, Glycerol electrooxidation on Pd modified Au surfaces in alkaline media: Effect of the deposition method, J Chem Phys. 150 (2019) 041703. https://doi.org/10.1063/1.5048489.

[33] A.N. Geraldes, D.F. da Silva, E.S. Pino, J.C.M. da Silva, R.F.B. de Souza, P. Hammer, E.V. Spinacé, A.O. Neto, M. Linardi, M.C. dos Santos, Ethanol electro-oxidation in an alkaline medium using Pd/C, Au/C and PdAu/C electrocatalysts prepared by electron beam irradiation, Electrochim Acta. 111 (2013) 455–465. https://doi.org/10.1016/j.electacta.2013.08.021.

[34] Y.M. Asal, A.M. Mohammad, S.S. Abd El Rehim, I.M. Al-Akraa, Preparation of Co-electrodeposited Pd-Au Nanocatalyst for Methanol Electro-oxidation, Int J Electrochem Sci. 16 (2021) 211133. https://doi.org/10.20964/2021.11.30.

[35] S.B. Strbac, M. Smiljanić, Z. Rakočević, S. Štrbac, Ethanol Oxidation on Pd/Au(111) Bimetallic Surfaces in Alkaline Solution, 2013. www.electrochemsci.org.

[36] T.R. Maumau, R.M. Modibedi, M.K. Mathe, Electro-oxidation of alcohols using carbon supported gold, palladium catalysts in alkaline media, 2018. www.sciencedirect.comwww.materialstoday.com/proceedings2214-7853.

[37] L.S. Aota, C. Jung, S. Zhang, S.-H. Kim, B. Gault, Revealing Compositional Evolution of PdAu Electrocatalyst by Atom Probe Tomography, ACS Energy Lett. 8 (2023) 2824–2830. https://doi.org/10.1021/acsenergylett.3c00911.

[38] S. Shen, Y. Guo, L. Luo, F. Li, L. Li, G. Wei, J. Yin, C. Ke, J. Zhang, Comprehensive Analysis on the Highly Active and Stable PdAu/C Electrocatalyst for Ethanol Oxidation Reaction in Alkaline Media, The Journal of Physical Chemistry C. 122 (2018) 1604–1611. https://doi.org/10.1021/acs.jpcc.7b10009.

[39] Y. Wang, N.S. Hush, J.R. Reimers, Simulation of the Au (111)- (22 x 3^(1/2) surface reconstruction, Phys Rev B. 75 (2007) 233416. https://doi.org/10.1103/PhysRevB.75.233416.

[40] D. Nečas, P. Klapetek, Gwyddion: an open-source software for SPM data analysis, Open Physics. 10 (2012). https://doi.org/10.2478/s11534-011-0096-2.

[41] I. Achari, S. Ambrozik, N. Dimitrov, Electrochemical Atomic Layer Deposition by Surface Limited Redox Replacement of Pd Thin Films in One-Cell Configuration Using Cu UPD Layers: Interrupting Mass-Transport Limited Growth, J Electrochem Soc. 165 (2018) J3074–J3082. https://doi.org/10.1149/2.0121815jes.

[42] S.R. Brankovic, J.X. Wang, R.R. Ad Zi, Metal monolayer deposition by replacement of metal adlayers on electrode surfaces, n.d. www.elsevier.nl/locate/susc.

[43] L.A. Kibler, Preparation and Characterization of Noble Metal Single Crystal Electrode Surfaces, 2003. http://www.uni-ulm.de/echem.

[44] J. Tang, M. Petri, L.A. Kibler, D.M. Kolb, Pd deposition onto Au(111) electrodes from sulphuric acid solution, Electrochim Acta. 51 (2005) 125–132. https://doi.org/10.1016/j.electacta.2005.04.009.

[45] W. Giurlani, E. Berretti, M. Innocenti, A. Lavacchi, Measuring the Thickness of Metal Coatings: A Review of the Methods, Coatings. 10 (2020) 1211. https://doi.org/10.3390/coatings10121211.

[46] A. Moy, J. Fournelle, BadgerFilm: An Open Source Thin Film Analysis Program, Microscopy and Microanalysis. 26 (2020) 496–498. https://doi.org/10.1017/S1431927620014853.

[47] F. D'Acapito, ESRF LISA Beamline (BM-08) Annual Report, (2017). https://www.esrf.fr/files/live/sites/www/files/UsersAndScience/Experiments/CRG/BM08/General/IT CRG%40ESRF Activity Report_2017.pdf.

[48] A. Puri, G. Lepore, F. d'Acapito, The New Beamline LISA at ESRF: Performances and Perspectives for Earth and Environmental Sciences, Condens Matter. 4 (2019) 12. https://doi.org/10.3390/condmat4010012.

[49] J.-L. Revol, P. Berkvens, J.-F. Bouteille, N. Carmignani, L. Carver, J. Chavanne, J.M. Chaize, F. Ewald, A. Franchi, L. Hardy, J. Jacob, G. Le Bec, I. Leconte, S.M. Liuzzo, L. Jolly, D. Martin, J. Pasquaud, T. Perron, Q. Qin, P. Raimondi, B. Roche, K.B. Scheidt, R. Versteegen, S. White European, ESRF-EBS: IMPLEMENTATION, PERFORMANCE AND RESTART OF USER OPERATION, (2021). https://doi.org/10.18429/JACoW-IPAC2021-THPAB074.

[50] A.P. Francesco d'Acapito, Giovanni Orazio Lepore, A.D.L. Alessio Laloni, Fabrizio La Manna, Eric Dettona, A. Martin, The LISA beamline at ESRF, (2019) 551–558. https://doi.org/10.1107/S160057751801843X.

[51] I. Davoli, H.N. Thanh, F. d'Acapito, ReflEXAFS technique: a powerful tool for structural study in new materials, in: AIP Conf Proc, AIP, 2003: pp. 388–394. https://doi.org/10.1063/1.1536400.

[52] F. D'Acapito, I. Davoli, P. Ghigna, S. Mobilio, The ReflEXAFS station at the GILDA beamline (BM08) of ESRF, J Synchrotron Radiat. 10 (2003) 260–264. https://doi.org/10.1107/S0909049503005582.

[53] D.M. Kolb, J. Schneider, Surface reconstruction in electrochemistry: Au(100-(5 × 20), Au(111)-(1 × 23) and Au(110)-(1 × 2), Electrochim Acta. 31 (1986) 929–936. https://doi.org/10.1016/0013-4686(86)80005-6.

[54] H. Aitchison, N. Meyerbröker, T.-L. Lee, J. Zegenhagen, T. Potter, H. Früchtl, I. Cebula, M. Buck, Underpotential deposition of Cu on Au(111) from neutral chloride containing electrolyte, Physical Chemistry Chemical Physics. 19 (2017) 24146–24153. https://doi.org/10.1039/C7CP04244B.

[55] C.H. Chen, K.D. Kepler, A.A. Gewirth, B.M. Ocko, J. Wang, Electrodeposited bismuth monolayers on gold (111) electrodes: comparison of surface x-ray scattering, scanning tunneling microscopy, and atomic force microscopy lattice structures, J Phys Chem. 97 (1993) 7290–7294. https://doi.org/10.1021/j100130a028.

[56] V. Rooryck, F. Reniers, C. Buess-Herman, G.A. Attard, X. Yang, The silver upd on gold(111) revisited, Journal of Electroanalytical Chemistry. 482 (2000) 93–101. https://doi.org/10.1016/S0022-0728(00)00002-4.

[57] M.A. Schneeweiss, D.M. Kolb, The Initial Stages of Copper Deposition on Bare and Chemically Modified Gold Electrodes, Physica Status Solidi (a). 173 (1999) 51–71. https://doi.org/10.1002/(SICI)1521-396X(199905)173:1<51::AID-PSSA51>3.0.CO;2-O.

[58] M. Nakamura, O. Endo, T. Ohta, M. Ito, Y. Yoda, Surface X-ray diffraction study of Cu UPD on Au() electrode in 0.5 M H2SO4 solution: the coadsorption structure of UPD copper, hydration water molecule and bisulfate anion on Au(), Surf Sci. 514 (2002) 227–233. https://doi.org/10.1016/S0039-6028(02)01634-5.

[59] Z. DURSUN, Ş.U. KARABİBEROĞLU, B. GELMEZ, A. BAŞARAN, Electrocatalytic oxidation of ethanol on various metal ad-layer modified Au(111) electrodes in alkaline solution, Turk J Chem. (2011). https://doi.org/10.3906/kim-1007-777.

[60] J. Torrero, M. Montiel, M.A. Peña, P. Ocón, S. Rojas, Insights on the electrooxidation of ethanol with Pd-based catalysts in alkaline electrolyte, Int J Hydrogen Energy. 44 (2019) 31995–32002. https://doi.org/10.1016/j.ijhydene.2019.10.124.

[61] W. Giurlani, M. Innocenti, A. Lavacchi, X-ray Microanalysis of Precious Metal Thin Films: Thickness and Composition Determination, Coatings. 8 (2018) 84. https://doi.org/10.3390/coatings8020084.

[62] W. Giurlani, E. Berretti, M. Innocenti, A. Lavacchi, Coating Thickness Determination Using X-ray Fluorescence Spectroscopy: Monte Carlo Simulations as an Alternative to the Use of Standards, Coatings. 9 (2019) 79. https://doi.org/10.3390/coatings9020079.

[63] W. Giurlani, E. Berretti, A. Lavacchi, M. Innocenti, Thickness determination of metal multilayers by ED-XRF multivariate analysis using Monte Carlo simulated standards, Anal Chim Acta. 1130 (2020) 72–79. https://doi.org/10.1016/j.aca.2020.07.047.

[64] E. Berretti, M.V. Pagliaro, A. Giaccherini, G. Montegrossi, F. Di Benedetto, G.O. Lepore, F. D'Acapito, F. Vizza, A. Lavacchi, Experimental evidence of palladium dissolution in anodes for alkaline direct ethanol and formate fuel cells, Electrochim Acta. 418 (2022) 140351. https://doi.org/10.1016/j.electacta.2022.140351.

[65] Berretti, Giaccherini, Montegrossi, D'Acapito, Di Benedetto, Zafferoni, Puri, Lepore, Miller, Giurlani, Innocenti, Vizza, Lavacchi, In-situ Quantification of Nanoparticles Oxidation: A Fixed Energy X-ray Absorption Approach, Catalysts. 9 (2019) 659. https://doi.org/10.3390/catal9080659.